Biogeosciences, 23, 21–38, 2026
https://doi.org/10.5194/bg-23-21-2026

Biogeosciences Open Access EGU

Archaeal lipostratigraphy of the Scotian Slope shallow sediments, Atlantic Canada

Narges Ahangarian[1], Unyime U. Umoh[1], Natasha MacAdam[2], Adam MacDonald[2], Patricia Granados[3], Jeremy N. Bentley[1], Elish Redshaw[1], Martin G. Fowler[4], Venus Baghalabadi[1,5], and G. Todd Ventura[1]

[1]Department of Geology, Saint Mary's University, 923 Robie Street, Halifax, Nova Scotia B3H 3C3, Canada
[2]Nova Scotia Department of Energy, 1690 Hollis St., Halifax, Nova Scotia B3J 3J9, Canada
[3]Centre for Environmental Analysis and Remediation, Saint Mary's University,
923 Robie Street, Halifax, Nova Scotia B3H 3C3, Canada
[4]Applied Petroleum Technology (Canada) Ltd., Calgary, AB T3A 2M3, Canada
[5]Department of Pharmacology, Dalhousie University, 5850 College St, Halifax, Nova Scotia, B3H 4R2, Canada

Correspondence: Narges Ahangarian (narges.ah@hotmail.com) and G. Todd Ventura (todd.ventura@smu.ca)

Received: 14 March 2025 – Discussion started: 28 March 2025
Revised: 28 October 2025 – Accepted: 1 November 2025 – Published: 5 January 2026

Abstract. The Scotian Slope in the North Atlantic Ocean extends for ∼500 km along the coast of Nova Scotia, Canada. Its surface sediments host microbial communities, which respond to complex geochemical drivers that not only include communication with the overlying water column, but also potential advection from deeper basinal fluids. Archaea are fundamental components of these communities, and their lipids act as important historical indicators of environmental geochemical change and microbial interactions within marine sediments. This study evaluates the spatial abundance and diversity of archaeal lipids preserved in shallow Scotian Slope sediments to better understand processes. Seventy-four sediment samples from 32 gravity and piston cores, reaching a maximum of 9 m below seafloor (m b.s.f.) were collected during three survey cruises. In total, 14 archaeal lipid classes comprising 42 unique compounds were detected. The lipid distributions reflect a high contribution of anaerobic methanotrophic (ANME) archaeal groups, such as ANME-1 to -3. Hierarchical cluster analysis and principal components analysis were used to show varying contributions of four lipid classes that included distinct assemblages of intact polar lipids (IPLs), core lipids (CLs), and their degradation products (CL-DPs). IPL to CL and CL to CL-DP turnover rates were estimated for the various lipid classes. Four stratigraphically distinct archaeal lipidomes were observed. The first, reflects a unique community influenced by a nearby cold seep. Three additional ambient sediment lipidomes were detected with overlapping depth intervals. These lipidomes contained varying abundances of IPL, CL, and CL-DPs, which likely mark geochemically controlled, microbial community variations that are further accompanied by a systematic increase to the stockpile of diagenetically altered lipids. The ambient sediment lipidomes appear to be highly spatially conserved across the latitudinal extent of the study area marking a resolvable shallow sediment lipostratigraphy that occupies a sediment stratigraphy that spans ∼27 000 ± 4000 years of basin evolution for the Scotian Slope.

1 Introduction

The Scotian Slope marks a portion of the North American continental shelf that extends for ∼500 km along the eastern coastal seaboard of Nova Scotia (Fig. 1). The slope descends from ∼400 m at the shelf edge to ∼5000 m water depth near the abyssal plain. Underlying this is a depositional history that began in the Late Triassic leading to 250 million years of continuous sedimentation (Wade and MacLean 1990). Large portions of the deeper sediment basin are affected by salt tectonism, which has greatly impacted basin stratigraphy and locally facilitated hydrocarbon seepage to the ocean seafloor. Deep basin salt tectonic movement has caused localized changes to the sub-basin stratigraphy at all depths resulting

the formation of minibasins and in the breaking of petroleum reservoir seals that have in some cases produced hydrocarbon seeps on the ocean floor (Campbell, 2019; Fowler et al., 2017; Bennett and Desiage, 2022; Chowdhury et al., 2024). How near surface sedimentary microbial ecosystems respond to their geochemical conditions especially when impacted by hydrocarbon seepage is not fully resolved.

The Scotian Slope is therefore an ideal region for examining the interplay between organic matter preservation and microbial interactions, both of which are critical to global carbon cycling. Genomic analyses, including 16S rRNA amplicon sequencing and metagenomic profiling, have resolved diverse microbial communities inhabiting surface and shallow sediments. Bacteria including Proteobacteria, Desulfobacterota, and Caldatribacteriota are the most abundant phyla across various strata (Zorz et al., 2023). Prominent lineages such as Gammaproteobacteria, Deltaproteobacteria, and Alphaproteobacteria are detected in the near surface with Atribacteria, Chloroflexi, and Deltaproteobacteria dominating deeper sediments (Dong et al., 2020). Of the archaeal domain, members of Thaumarchaeota (more recently reclassified as Nitrososphaerota, Rinke et al., 2021) dominate the shallow and surface sediments with decreasing abundance in deeper strata, while phyla such as Methanomicrobia and Lokiarchaeota mark the dominant taxa in deeper buried sediments (Dong et al., 2020). Archaeal communities such as ANME-1 and ANME-2, which play important roles in the anaerobic oxidation of methane, are prominent at depths corresponding to the sulfate-methane transition zone (Dong et al., 2020). The metabolic specificity of these organisms alongside their community composition can be strong indicators of hydrocarbon seepage at targeted Scotian Slope sites (Dong et al., 2020; Li et al., 2023). For example, microbial communities capable of oxidizing C2+ alkanes dominate the shallow sediments of these hydrocarbon seeps (Zorz et al., 2023). Additionally, microbial communities in sediments close to cold seeps can be enriched in thermophilic bacterial endospores, which produces an influx of deeper biosphere microfauna into the shallow marine sedimentary environment (Gittins et al., 2022; Rattray et al., 2023). As such, the complex microbial communities inhabiting these sediments are characterized as being depth stratified and further influenced by hydrocarbon seepage (Li et al., 2023).

Deep marine sediments are globally extensive, complex, and dynamic biogeochemical interfaces, which serve as sinks for carbon and nutrients (Burdige, 2007). The interaction between microbial communities and sedimentary processes within these environments is a key component of nutrient cycling, organic matter degradation, and environmental changes over geological timescales (Orcutt et al., 2011). A major microbial driver of these processes are archaea, which are ubiquitous in deep marine sediments (Sturt et al., 2004; Fredricks and Hinrichs, 2007; Lipp et al., 2008; Hoshino et al., 2020; Lipp and Hinrichs, 2009; Biddle et al., 2006). Archaea play critical roles in the transformation of carbon and nitrogen (Offre et al., 2013). Their ability to adapt to diverse and extreme conditions makes them important subjects in the study of life's extremes and global ecological processes (Valentine, 2007; Sollich et al., 2017).

The unique membrane lipid structures of archaea differ from bacteria and eukarya (e.g., Koga et al., 1993; De Rosa, 1996). Archaeal membrane lipids consist of isoprenoidal hydrocarbon chain to the glycerol backbone through ether bonds (De Rosa, 1996). Intact polar lipids (IPLs) such as phospholipids, glycolipids, and ornithine lipids with polar headgroups that can potentially indicate active, or recently active, microbial cells (Sturt et al., 2004; Lipp and Hinrichs, 2009; Schouten et al., 2010, 2013). In contrast, core lipids (CLs) can be degraded remnants of IPLs where they are then informative of past microbial community dynamics (White et al., 1979) or are the intermediate products of lipid biosynthesis in living cells (Liu et al., 2012a; Meador et al., 2014; Villanueva et al., 2014). Therefore, variation between CLs and IPLs can indicate shifts in microbial community structure and function with sediment depth by diagenesis (Biddle et al., 2006; Schouten et al., 2013). The composition and distribution of lipid biomarkers, particularly IPLs and CLs, are important in studying marine sediments for tracing microbial life and environmental conditions (Koelmel et al., 2020). The unique compounds such as glycerol dialkyl glycerol tetraethers (GDGTs) can serve as indicators of archaeal activity and in reconstructing past environmental conditions, in terms of the strength of ammonia oxidation, changing sea surface temperature, methane cycling, and pH variations of soils (e.g., Schouten et al., 2002; Kim et al., 2010; Zhang et al., 2011; Hurley et al., 2016; Xiao et al., 2016; Guan et al., 2016).

For this study, the diversity and abundance of archaeal lipids extracted from shallow ocean floor sediments of the Scotian Slope are examined to provide further insights into the microbial processes of deep marine sedimentary systems. The resolvable assemblages of archaeal lipids, referred to here as lipidomes, are examined across three spatial dimensions: sediment depth, distance down the continental slope, and along $\sim 3^{\circ}$ latitude change of the northwestern trend of the continental margin. They are then compared with several sedimentological, geochemical, and archaeal lipid proxy ratios to better constrain the microbial community structure and function within the sediments as well as to improve constraints on their diagenetic alteration rates.

2 Materials and methods

2.1 Sample collection

Seventy-four sediment samples were selected from 32 piston and gravity cores collected during three survey cruises that took place aboard the CCGS *Hudson* research vessel in 2015, 2016, and 2018 (Fig. 1 and Table S1 in the Supple-

ment). The total area covered was $\sim 40\,000\,km^2$, marking $\sim 3°$ of latitudinal, and ~ 1500 to 3500 m variation to the ocean depth. Of these, 17 sediment samples were acquired from 12 piston cores during the 2015 expedition. Twenty-four sediment samples were taken from 16 piston cores during the 2016 cruise, and 33 sediment samples were obtained from four gravity cores during the 2018 cruise. A 10 m piston corer was used for the 2015 and 2016 cruises (Campbell and MacDonald, 2016; Campbell, 2019). The 2018 cruise used a gravity corer that extended to 6 m in length. All cores were immediately sectioned into 1.5 m long intervals on-board the ship and inspected for diagnostic signs of hydrocarbon seepage (e.g., gas cracks, bubbling, or strong odours; Campbell and Normandeau, 2019). Sediment within 20 cm of the base of each core was scooped into a 500 mL IsoJar (Isotech Laboratories, Inc.), flushed with nitrogen, sealed, and stored at −20 °C for hydrocarbon biomarker and headspace gas analyses (Fowler et al., 2017). The remaining full-length cores were then split longitudinally with a core splitter and further inspected for lithology, obvious hydrocarbon staining, and evidence of gas. Samples for geochemical analyses were wrapped in aluminium foil, sealed in Whirl-pack® bags, and frozen at −80 °C on board the ship. These samples were kept frozen until analysed at the land-based laboratories. Information regarding the specific sampling sites is available in cruise reports (Campbell and MacDonald, 2016; Campbell, 2019; Campbell and Normandeau, 2019). Among these samples, core "2018, 0007" (Table S1) collected from a gravity core that targeted a suspected cold seep site (Campbell and Normandeau, 2019) appears to have been impacted by hydrocarbon seepage based on additional geochemical evidence (Fowler et al., 2017). Several other cores had sediment intervals potentially indicating the presence of hydrocarbons (Table S2) that were far away from the sampled intervals investigated in this study. Lithologic information was extracted from the open file cruise report Jenner et al. (2022) for core samples collected on 2015 expedition cruise. Sediment lithologic information for the other samples was provided by GSC Atlantic, NRCAN for cores collected during the 2016 and 2018 expedition cruises and are recorded in Table S2.

2.2 Bulk sediment geochemistry

Approximately 10 g of the frozen sediment was weighed, desiccated in a drying oven at 30 °C, and reweighed to obtain its dry weight. The dried sediment was powdered using a mortar and pestle and acid digested in 6N H_3PO_4 solution for 4 d. Once the inorganic carbon was removed, the sediment was flushed with Milli-Q water, transformed into a slurry using a vortex mixer, and centrifugated at 1250 rpm for 7 min. The supernatant was decanted and the process was repeated until the sediment was renormalized. Decarbonated sediments were then subsampled for bulk geochemical analysis to constrain organic matter source and diagenetic changes with sediment depth. Sediment total organic carbon

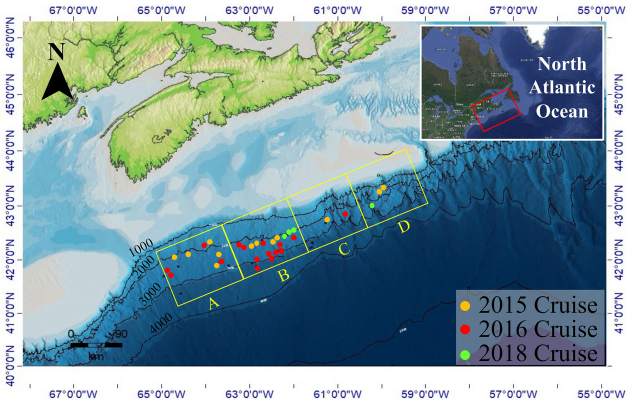

Figure 1. ArcGIS bathymetric map of the North Atlantic Scotian Margin displaying piston and gravity core locations used in this study. Core locations are grouped into four equal area quadrants (labelled A–D) that extend parallel along the Scotian Slope. Colour circles mark the year that the survey cruise was conducted.

(TOC) and total nitrogen (TN) was measured using a Perkin-Elmer 2400 Series II CHNS/O Elemental Analyzer (EA) located in the Centre for Environmental Assessment and Remediation at Saint Mary's University. Stable carbon isotope of TOC ($\delta^{13}C_{TOC}$) measurements were obtained from the University of Calgary.

2.3 Porewater Geochemistry

Porewater was extracted from sediments using Rhizon samplers and by centrifugation at 2500 rpm for 10 min. The porewater was decanted into a pre-combusted glass beaker, then filtered through a 0.45-µm filter to remove sediment particles. The exact volume of extracted porewater was recorded as a measure of sediment porosity. Porewater anion concentrations were measured using a Thermo Scientific Dionex Aquion Ion Chromatography Conductivity Detector System with an anion-exchange column and a DS6 Heated Conductivity Cell fitted with an AERS_4 mm suppressor pump and a Dionex AXP Auxiliary pump and pump ECD from the Saint Mary's University Organic Geochemistry Laboratory (OGL). The IC was further configured with an in-line Thermo Scientific 9 × 24 mm Dionex InGuard Ag sample prep cartridge and Thermo Scientific Dionex InGuard Na prep cartridge to facilitate trace analysis of seawater. The system was controlled via Thermo Scientific Chromeleon 7 chromatography system version 7.3 software. Seven Anion Standard II (from Sunnyvale, California) in deionized water. The anion standard (S+D) was an amalgamation of H_2O (99.9 %, CAS# 7732-18-5) and the following anions – F^- (20 mg L^{-1}, CAS# 7681-49-4); Cl^- (100 mg L^{-1}, CAS# 7647-14-5); NO_2^- (100 mg L^{-1}, CAS# 7632-00-0); Br^- (100 mg L^{-1}, CAS# 7647-15-6); NO_3^- (100 mg L^{-1}, CAS# 7631-99-4); PO_4^{3-} (200 mg L^{-1}, CAS# 7778-77-0); SO_4^{2-} (100 mg L^{-1}, CAS# 7757-82-6), stored in −4 °C refrigera-

tor. Carbonate and Sulfite are prepared as separate stock solutions. Carbonate is prepared using Anhydrous Sodium Carbonate ACS powder from Fisher Chemicals (CAS # 497-19-8) and SO_3^{2-} is prepared using Anhydrous Sodium Sulfite crystalline powder from Fisher Chemicals (CAS# 7757-83-7). A seven-anion standard mixture was diluted to 0.5, 1, 2, 5, 10, 20, and 50 ppm to generate an external calibration curve. The high salinity of marine porewater requires that the system be equipped with two in-line guard cartridges to remove chloride (Cl^-) and sodium (Na^+) ions from the sample before reaching the anion-exchange column.

2.4 Lipid extraction

Before extraction, PAF (1-alkyl-2-acetyl-sn-glycero-3-phosphocholine) was added as a recovery standard into the samples. Total lipid extracts (TLE) were recovered with a modified Bligh and Dyer extraction technique (Bligh and Dyer, 1959; Sturt et al., 2004) as described in Bentley et al. (2022). The liquid-liquid extraction method employed a blend of polar and non-polar solvents that effectively separates the organic phase from the inorganic phase, while gently lysing cellular membranes.

2.5 Lipid separation and identification

Aliquots comprising 1 % and 3 % of the TLE were injected into an Agilent Technologies 1290 Infinity II ultra-high performance liquid chromatograph (UHPLC) coupled to a 6530-quadrupole time-of-flight mass spectrometer (qToF-MS) run in reverse phase using electrospray ionization. Liquid chromatographic separation used a ZORBAX RRHD Eclipse Plus C18 (2.1-mm × 150-mm × 1.8-µm) reverse phase column, equipped with a guard column, and maintained at a stable temperature of 45 °C throughout the sample analysis. The injection solvent was methanol. The mobile phase flow rate was set at 0.25 mL min^{-1} with the composition of mobile phases being methanol/formic acid/ammonium hydroxide ([100 : 0.04 : 0.10] $v : v : v$) for mobile phase A, and propan-2-ol/formic acid/ammonium hydroxide ([100 : 0.04 : 0.10] $v : v : v$) for mobile phase B. The mobile phase composition began with 100 % A for 10 min, stepped to a linear addition of B to 24 % held for 5 min, followed by a linear gradient to 65 % B for 75 min, then 70 % B for 15 min, that completed by re-equilibrating with 100 % A for 15 min.

Compounds were tentatively identified by mass spectral analysis in conjunction with expected chromatographic elution patterns (Table S3) as found in the literature (e.g. Wörmer et al., 2013, 2015; Yoshinaga et al., 2011; Schouten et al., 2008; Schubotz et al., 2009; Liu et al., 2012a). Lipid quantification used C_{21}-PC (1, 2-diheneicosanoyl-*sn*-glycero-3-phosphocholine) as an internal standard and was based on accurate mass detection of $[M^{\cdot}+H]^+$, $[M^{\cdot}+NH_4]^+$, and $[M^{\cdot}+Na]^+$ adducts using Agilent Technology Mass Hunter software. Lipids concentrations were then normalized to extracted sediment mass (µg g sed^{-1}) and sample TOC mass (µg wt% TOC^{-1}).

2.6 Calculation of adjusted TOC concentrations for lipid normalization

Organic matter systematically decreases by diagenetic processes as sediments become more deeply buried (e.g. Berner, 1980; Middelburg, 2019; Wallmann et al., 2006; Arndt et al., 2013). These changes result in a sediment depth bias for TOC normalized lipid concentrations. To account for this, each sample was corrected to an estimated-prediagenetically altered value based on a regression model adapted from the regionalized Scotian Slope sediment TOC depth profile (Fig. 2). The depth profile extended to 8.71 m b.s.f. as calculated from the 72 samples (after the removal of two outliers) collected from this study as well as 8 additional shallow sediment samples (< 1 m) from other ambient sediments. The inferred TOC value at depth i ($TOC_{adjusted_i}$) marking the original point in time of sediment deposition was calculated as the sum of a sample's measured TOC ($TOC_{measured_i}$) plus its predicted decayed ($TOC_{decayed_i}$) value following Eq. (1):

$$TOC_{adjusted_i} = TOC_{measured_i} + TOC_{decayed_i}, \quad (1)$$

The $TOC_{decayed_i}$ value was inferred using the organic matter decay curve calculated from the regionalized Scotian Slope sediment TOC depth profile (Fig. 2 and Eq. 2).

$$y = -406.6 \ln\left(TOC_{measured_i}\right) + 2.7102 \quad (2)$$

The regression model was then used to predict a regionalized reference TOC value ($TOC_{predicted}$) for any depth (y) within the study (Eq. 3).

$$TOC_{predicted_i} = e^{\frac{2.7102-y}{406.6}} \quad (3)$$

Because the TOC decay rate (n) varies with sediment depth, its value is determined across 1 m burial depth intervals (y) following Eq. (4):

$$f(n_i) = \frac{d(TOC_{predicted_i})}{dy_i} = -\frac{TOC_{predicted_i}}{366.2}, \quad (4)$$

where n_i is the TOC decay rate at depth i. The $TOC_{decayed}$ and $TOC_{adjusted}$ were then calculated at each depth using Eq. (5)

$$TOC_{decayed_i} = \sum_1^i \left(n_i \times TOC_{predicted_{i-1}}\right), \quad (5)$$

and Eq. (1) respectively and following the modelled TOC decay rate in Eq. (5) (Table S4 and Fig. S1).

2.7 Statistical analysis

A hierarchical cluster analysis (HCA), heatmap dendrogram of the sediment sample lipids, was generated with the R statistical software environment using the "heatmap" function

of the "gplots" package. Lipid abundances were transformed to their respective z-scores that then served as the data matrix. *Ward's* minimum variance unbounded distance function was applied to calculate the dissimilarity of the data matrix. Matrix cells were coloured according to a gradient scale representing the z-scored values. Minitab statistical software was then used to perform principal components analysis (PCA). PCA was performed on the lipid concentration data, which was transformed to a correlation matrix using a Mahalanobis distance, that was then used to calculate the centroid from the covariance structure of the data.

3 Results

3.1 Bulk sedimentary organic matter and porewater geochemistry

Sedimentary organic carbon ranged from 0.12 wt % to 1.1 wt % with an average of 0.5 wt % (Fig. 2 and Table S1). This was calculated based on 85 TOC measurements produced from 33 sediment cores. A sharp down core decrease in TOC is observed from 0 wt % to 0.5 m b.s.f., which is followed by a more gradual decrease with core depth. The TN values ranged from 0 wt % to 0.12 wt % with an average of 0.07 wt % (Fig. 2 and Table S1). Samples "2016-049, 443–448 cm" and "2015-029, 490–495 cm" comprise the lowest and highest TN values, respectively. The $\delta^{13}C_{TOC}$ values range from -21.7 to -24.4 ‰ (Fig. 2 and Table S1), with one outlier (-27.4 ‰ collected from seep site core "2018, 0007"). Collectively, these trends are consistent with shallow marine sediments experiencing early diagenetic alteration of its organic matter. The trends also indicate that while mass transport deposits likely have occurred within the upper 9 m of the sampled sediments, the impact has not changed the average organic matter loading profile of the slope.

Porewater anion measurements were conducted from 7 gravity and piston cores. The porewater anion concentrations were measured to capture carbon, nitrogen, and sulfur biogeochemical cycling. Low nitrate concentrations (~ 0.1 to ~ 0.2 mmol L^{-1}) steadily decrease over the 8m sediment depth (Fig. 2). Even lower nitrite concentrations (~ 0.05 to ~ 0.14 mmol L^{-1}) show an antiparallel trend and slightly increase with sediment depth. Dissolved inorganic carbon (DIC) steadily increased with depth (from near zero to ~ 8 mmol L^{-1}). An inverse sulfate depletion trend occurs with sediment depth (~ 28 to ~ 10 mmol L^{-1}). Together these sulfate and DIC mark the most dominant porewater geochemical feature that enables the identification of the sulfate alkalinity transition zone (SATZ). For the Scotian Slope, the SATZ resides at ~ 3.25 m b.s.f. This zone stratigraphically sits above the sulfate methane transition, which was not measured in this study.

3.2 Diversity of archaeal lipids in the Scotian Slope sediments

A total of 14 archaeal lipid classes comprising 42 unique compounds were tentatively identified and quantified across 74 sediment samples using mass spectrometric techniques and comparisons of elution times from the literature (Fig. 3 and Table S3). Lipid classes were grouped based on the hypothesized degree of preservation into IPLs, CLs, and CL-DPs. Additionally, upper water column plant and algae-based chlorophyll-*a* (Chl-*a*) and hydroxy-chlorophyll-*a* (OH-Chl-*a*) were identified and quantified as outgroup allochthonous additions to the seafloor.

Of these, eight IPL classes comprising 18 unique compounds were identified (Fig. 3 and Table S5). Detected monoglycosidic GDGTs (1G-GDGTs) comprising 0–3 rings and crenarchaeol (Cren). For this series 1G-GDGT-0 and 1G-Cren were the most abundant compounds. For di-glycosidic-GDGTs (2G-GDGTs), compound classes included 0–2 rings and Cren, with the acyclic lipid being the dominant compound. Detected hydroxylated 1G-GDGTs (1G-OH-GDGTs) were -0 to -2, with 1G-OH-GDGT-0 being the dominant compound. Hydroxylated 2G-GDGTs (2G-OH-GDGTs) ranged from 0–2 with the dominant compound also being 2G-OH-GDGT-0. Apart from monolayer lipid structures, four C_{40} bilayer IPLs were detected. These included mono- and di-glycosidic (1G- and 2G-ARs), phosphatidicacid, (PA-AR), and hydroxyphosphatidicacid (PA-OH-AR) archaeols.

Six classes of CL and CL-DPs comprising 24 unique compounds were identified (Fig. 3 and Table S6). Commonly detected GDGTs were GDGT-0 to GDGT-3, Cren, and the stereoisomer of crenarchaeol (Cren') (Liu et al., 2018; Sinninghe Damsté et al., 2018). For these compounds, GDGT-0 and Cren were the most abundant archaeal lipids in the surveyed region of the Scotian Slope sediments. Detected hydroxyl glycerol dialkyl glycerol tetraethers (OH-GDGTs) comprised OH-GDGT (0–3, and Cren) with OH-GDGT-0 being the dominant compound were also observed in all surveyed samples. Archaeol was detected in all sediment samples, where it typically marked the third most abundant archaeal lipid on most sediment samples (Fig. 3 and Table S5).

Archaeal CL-DPs take on many forms (e.g., Liu et al., 2016). For this study, only 13 derivatives were targeted. These putatively include the glycerol dialkanol diethers (GDDs) 0–4 and Cren, with GDD-0 and GDD-Cren being the dominant compounds; hydroxylated glycerol dialkanol diethers (OH-GDDs) 0–2, dominated by OH-GDD-0; and biphytanic diols 0–3 (BpDiols) with BpDiol-0 being the most prevalent highly degraded archaeal biomarker (Fig. 3 and Table S6).

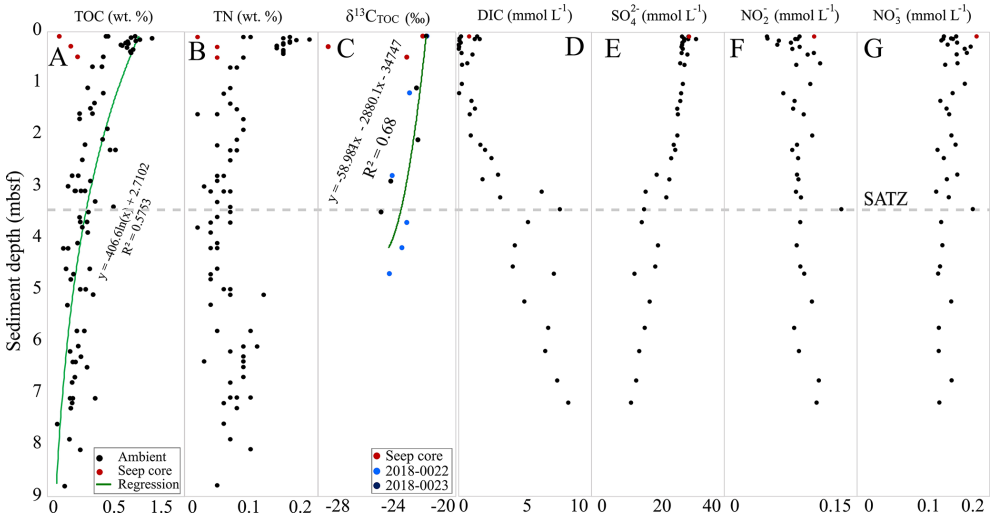

Figure 2. Down core TOC, TN, DIC, pore water anions, and stable carbon isotope ($\delta^{13}C_{TOC}$) trends of the Scotian Slope sediment samples. Dotted line indicates the SATZ.

4 Discussion

4.1 Chemotaxonomic relationships

Details on the chemotaxonomic relationships of the resolved Scotian Slope archaeal lipids can be found in the Supplement.

4.2 Regional sediment depth trends

Lipid concentrations from sediment samples were binned into 1 m thick stratigraphic intervals to derive regional down-core depth trends (Fig. 4A–L). The sediment and TOC normalized concentrations of IPLs, CLs, CL-DPs, and upper water column photosynthetic pigments were then averaged across all samples falling into its specific depth interval (Figs. 4 and S2). The 14 lipid classes have distinct trends with both increasing and decreasing loadings with sediment depth that are further complicated by occasional lack of consistency between the two normalization schemes. These variations strongly suggest the lipid class are derived from different source inputs.

Resolving archaeal lipid source inputs is difficult and the subject of long-term disagreement (e.g., Zhang et al., 2011; Hu et al., 2015; Li et al., 2016; Guo et al., 2018; Cheng et al., 2021; Umoh et al., 2022). For this study, sourcing considers the following framework. Comparisons between the two lipid normalization methods enable a basic premise for determining allochthonous versus autochthonous input. This is because normalization by sediment TOC adjusts the lipid concentration relative to what is largely an allochthonous input of upper water column supply of detrital sedimentary organic matter. Alternatively, because the ocean floor sediments contain relatively low organic matter abundances (< 1.1 wt %) the method of normalizing lipid concentrations to sediment volume imparts little influence from upper primary productivity. Therefore, when these two normalization schemes produce similar depth trends, the quantified lipid is likely derived from the overlying water column. However, if dissimilar down core profiles are found the lipid is more likely to have been sourced from within its host sediment. Additionally, euphotic zone produced photosynthetic pigments, Chl-*a* and OH-Chl-*a*, should also provide a stratigraphic record of changing productivity through time. These pigments alternate between high and low loadings and have near identical depth trends across both normalization methods (Fig. 4L). We therefore interpret other lipid classes as being largely sourced from the upper water column if: (1) their down-core profiles are the same across both normalization schemes and (2) their stratigraphic loadings match the measured Chl-*a* and OH-Chl-*a* depth profiles (Fig. 4L). We further interpret lipid classes as being sourced within the sedimentary environment if sediment normalized depth trends dominate over their respective TOC normalized counterparts.

Normalized down core concentration profiles suggest 1G-GDGTs and GDGTs -0, -1, and -Cren are largely dominated by upper water column inputs as their two normalized stratigraphic trends largely replicate the photosynthetic pigment profile (Fig. 4A and F). However, an additional input of sedimentary-sourced lipids appears to arise over the 5 to 9 m depth range. 2G-GDGTs appears to be sourced from within the upper 0–3 m b.s.f. of sediments (Fig. 4C) as neither normalization profile matches Chl-*a* and the mean lipid concentration at 1 m much greater than what is observed for all other depths. 1G-OH-GDGT-0, -1, and -2 appear to be sourced from the water column as their TOC normalized abundances are largely weighted to the TOC normalization method for these intervals (Fig. 4B). Additionally, similar to their IPL precursors, OH-GDGTs appear to be sourced

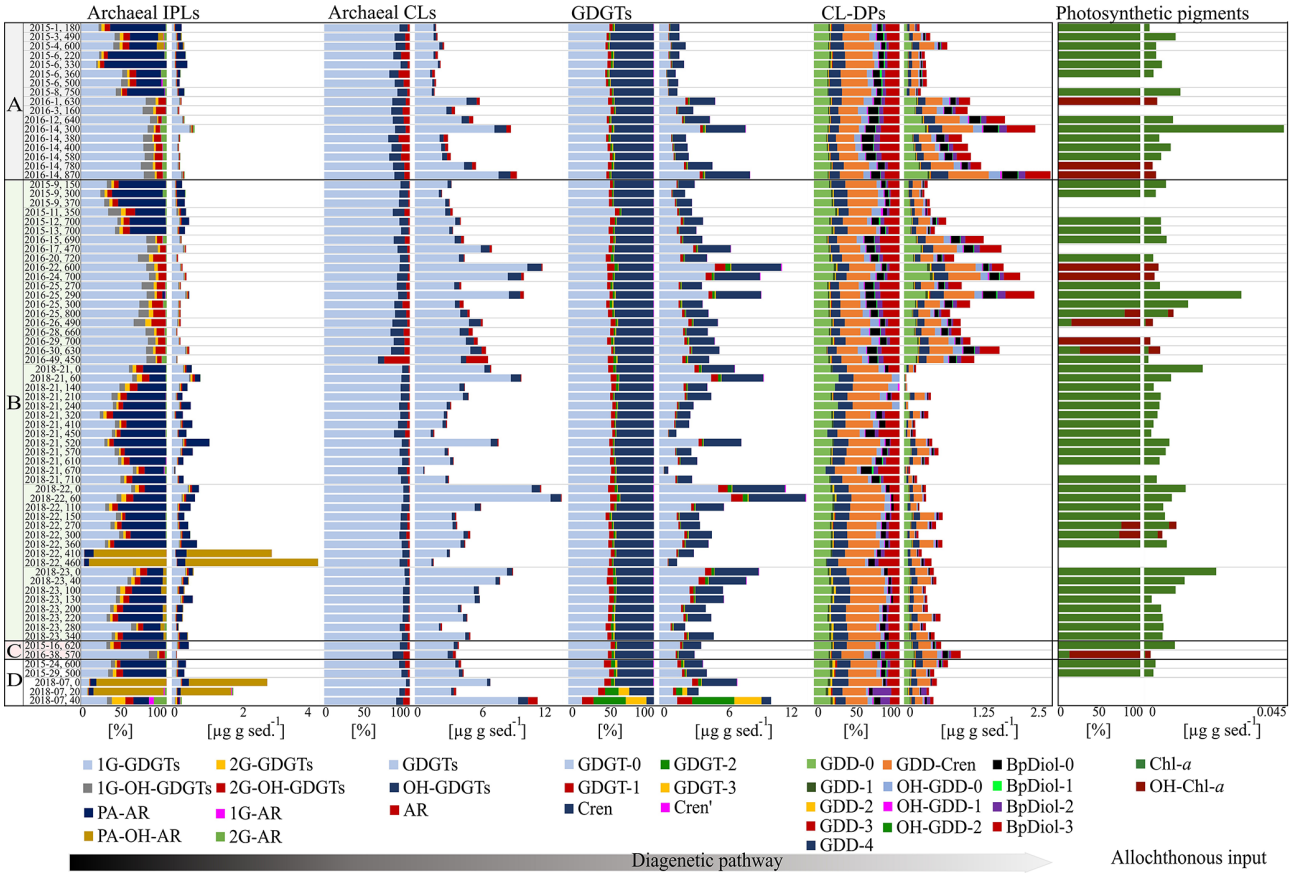

Figure 3. Relative and absolute abundances of archaeal IPL, CL, CL-DP, and photosynthetic pigments within the four Scotian Slope quadrants (A–D; Fig. 1) core sediments (sample data provided in Table S1).

from the water column as the compounds have more dominant TOC normalized abundances. IPL-based ARs appear to be largely sourced from sediments as their abundances are distinctly different from that of the photosynthetic pigments down core trends and are dominated by sediment normalized concentration trends (Fig. 4H). For CL-DPs, the larger TOC normalized contributions of GDDs, OH-GDDs, and BpDiols suggests these compound's precursors were largely derived from the water column (Fig. 4I–K). In summary, water column loading is the main source for 1G-GDGTs in the Slope. 2G-GDGTs, OH-GDGTs, ARs, and CL-DPs have a mixed source, but largely derived from within the ocean floor sediments. As much of the quantified lipid classes arise from the water column and the near surface, they are potentially prone to being diagenetically altered with time as they become more deeply buried.

4.3 Preservation potential of archaeal lipids

Intact polar membrane lipids, especially IPL-GDGTs, have been used as biomarkers for living microbial communities in marine sediments (Biddle et al., 2006; Lipp et al., 2008; Schubotz et al., 2011; Rossel et al., 2011; Xie et al., 2014; Evans et al., 2017; Carr et al., 2018) under the assumption that these compounds rapidly degrade to CLs upon cell death. Detected IPLs in sediments were therefore considered to be produced by in situ microbial communities. However, degradation models of sedimentary IPLs indicate that there may also be substantially IPL contributions to fossil compounds as these compounds can be preserved across geological time scales (Lipp and Hinrichs, 2009; Schouten et al., 2010; Lengger et al., 2013, 2014 Lin et al., 2013; Xie et al., 2013; Wu et al., 2019), showing that they are not accurate biomarkers for living microbial biomass. Moving beyond the initial stages of IPL alteration is the prospect that CLs will degrade to other more chemically simple alteration products. Among these are GDDs, which are ubiquitously found in marine sediments (Knappy and Keely, 2012) and are generally known as GDGT degradation products (Liu et al., 2012c; Coffinet et al., 2015; Mitrović et al., 2023; Hingley et al., 2024). Because of their chemical structure, both sources of GDGT biosynthesis intermediates compounds (Liu et al., 2012a; Meador et al., 2014; Villanueva et al., 2014) and GDGTs degradation products (Knappy and Keely, 2012; Liu et al., 2012a; Yang et al., 2014) have been proposed. However, GDDs have been reported to have similar microbial origin to GDGTs rather

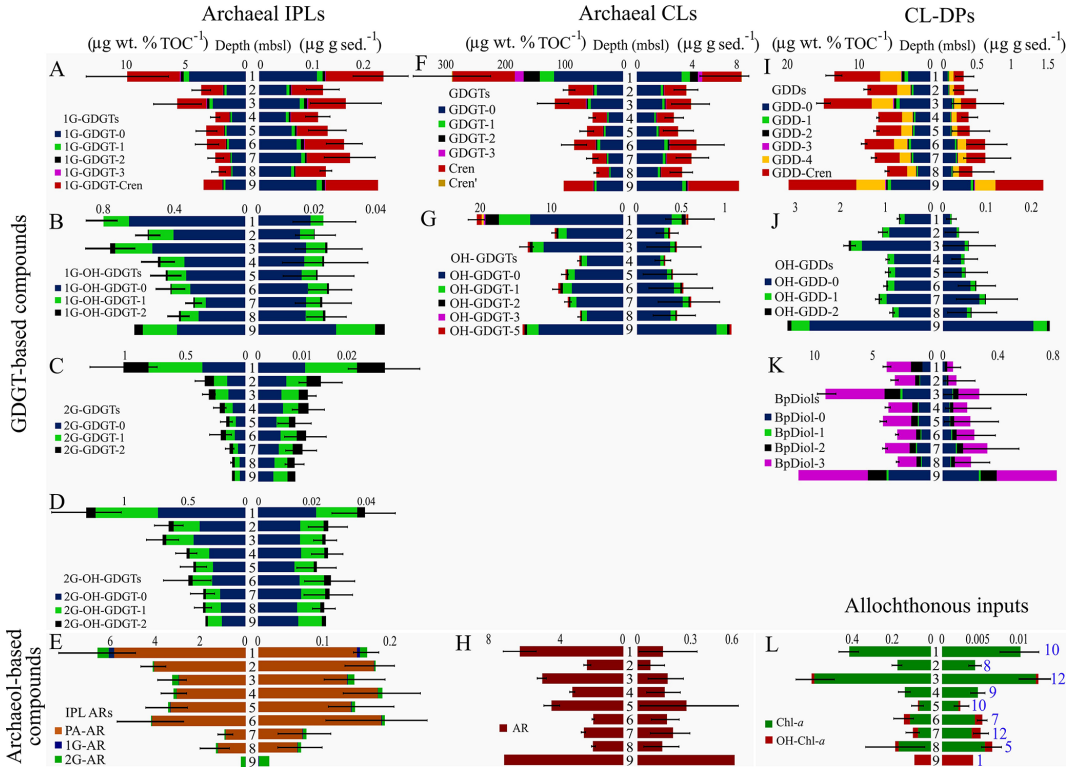

Figure 4. Bar graphs of down-core archaeal lipid class abundances normalized to sediment (right) and TOC (left) (blue font number in lower right bar graph indicates the summed samples for each depth interval). Black lines through the bars of each graph mark standard deviations of lipid abundance measurements.

than being a direct diagenetic product of them (Mitrović et al., 2023).

A simple diagenetic alteration pathway is therefore examined to help resolve lipid sourcing relationships (Fig. 5A–D) based on the structural complexity of various lipid classes. Lipid abundances were compared to test whether the model conforms to the conditions measured within the slope. A moderate correlation was found between the occurrence of 1G-GDGTs and GDGTs ($R^2 = 0.48$; Fig. 5A), which could arise from additional lipid incorporation within the sediments (see Sect. 4.2). It may equally derive from different living archaeal communities that host both IPL and CLs as part of their membrane structures (e.g. Ingalls et al., 2012), as well as a lack of diagenetic alteration owing to the recalcitrant nature of glycosidic headgroups (Lipp and Hinrichs, 2009; Wu et al., 2019; Bentley et al., 2022). Similarly, a moderate correlation also exists between GDGTs and GDDs ($R^2 = 0.59$ Fig. 5B; for the continuous series of lipidomes A3 and A4s that marks a continuous deeper sediment interval; see Sect. 4.5). GDGT sources do not directly lead to BpDiol production ($R^2 = 0.05$, Fig. S3). Instead, BpDiol appears to be almost exclusively sourced from GDDs ($R^2 = 0.75$; Fig. 5D).

As several structurally related lipid classes may be genetically related, mean slope degradation proxies (Eqs. 6–17; Table S7) were calculated and plotted as 1 m interval depth profiles (Fig. 6A–E). From these data, 1G-GDGTs and OH-GDGTs are not only observed to be quite resilient within the sedimentary environment; they may also have increased relative IPL concentration across different sediment depth intervals (Fig. 6A). Lipids with 2G headgroups appear to be less stable with a ~ 0.3 (for 2G-GDGT) and a 0.5 % (for 2G-OH-GDGT) per meter headgroup loss rates (Table S8; Fig. 6B). GDGTs are observed to transform to GDDs at a rate of 1.4 % m^{-1} (with a similar 1.6 % rate for OH-GDGTs). GDDs appear to systematically give rise to BpDiols (Fig. 6D). Following this general profile, there is an 18.3 % turnover in the GDDs pool relative to BpDiols from the surface to the bottom portion of the sediment profile, marking a 2 % m^{-1} transformation rate with sediment burial (Table S8). PA-AR, 1G-AR, and 2G-AR also appear to systematically degrade to AR at 7 % m^{-1}, 0.4 % m^{-1}, and 0.5 % m^{-1}, respectively. These results indicate the diagenetic alteration of lipids occurs, for most lipid classes following expected degradation paths over the $\sim 27 \pm 4$ Kyr (Jenner et al., 2022; Table S1; Fig. S4) interval that marks the 9 m surveyed depth of the Scotian Slope. The rate of change differs by the chemical structure with C80 structures having the following stability trends CL-DP (GDD) to CL-DP (BpDiol) $\gg$ CL to CL-DP > IPL to CL. C40 lipids follow a slightly different behavior with IPL-AR

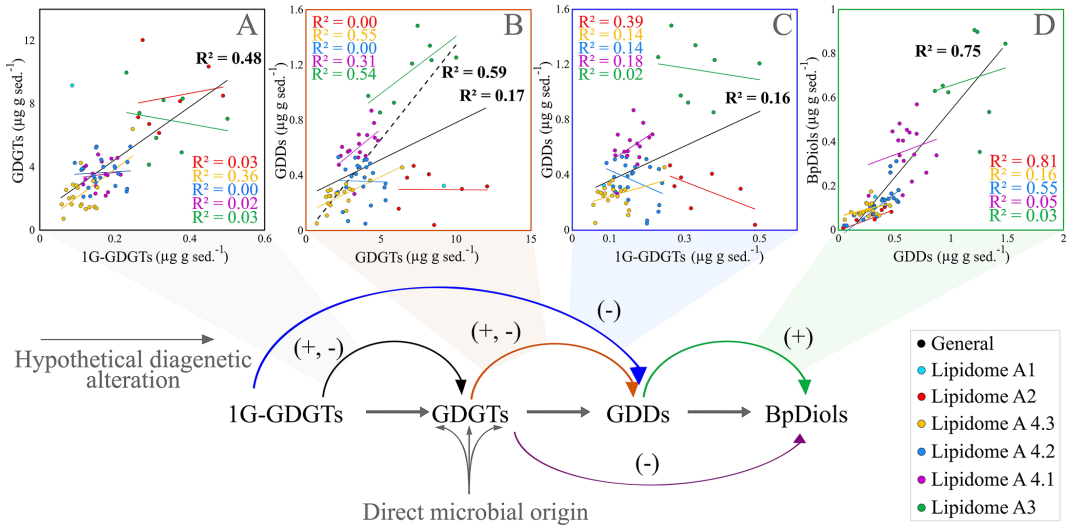

Figure 5. Cross plots of various lipid class concentrations associated within an expected diagenetic alteration pathway (bottom flow chart). Parentheses with plus and minus signs indicate statistically relevant agreements to the pathway. Lipidomes in the legend are discussed in Sect. 4.5.

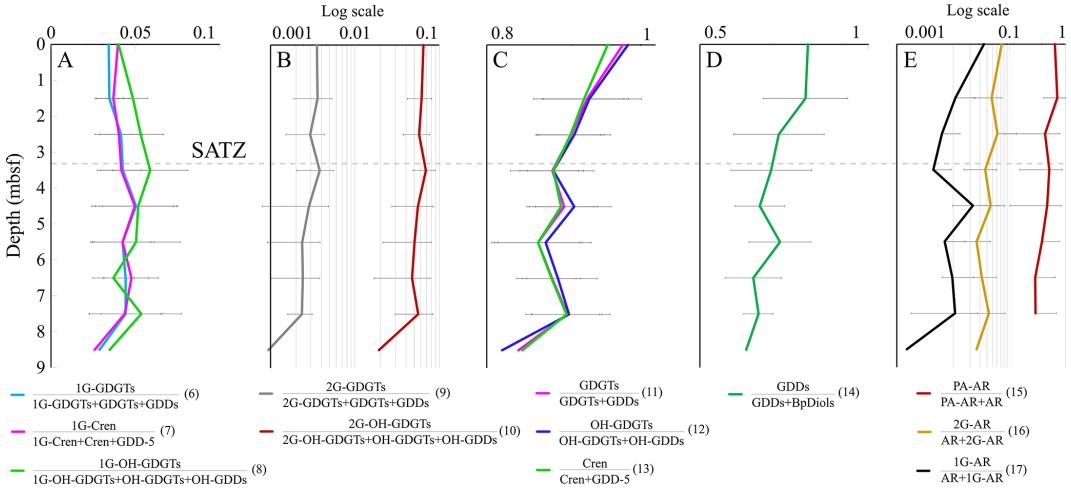

Figure 6. Lipid precursor to product pair changes with core depth. Dotted line indicates the SATZ. Numbers in parentheses label Eqs. (6)–(17).

(PA) to CL (AR) ≫ IPL-AR (1G & 2G) to CL (AR) (Table S8).

4.4 Archaeal lipid proxies for methane seepage

Sediments impacted by hydrocarbon seepage typically have unique microbial communities that include ANMEs (i.e., Boetius et al., 2000; Hinrichs et al., 2000; Pancost et al., 2001; Knittel and Boetius, 2009). To investigate this, downcore profiles of three archaeal lipid proxies were calculated for both CLs and IPLs to further elucidate the biogeochemical processes influencing lipid distributions (Fig. 7; Table S7). Of these, the methane index (MI; Eq. 6) (Zhang et al., 2011; Guan et al., 2016) measures the proportion of ANME-1 Euryarchaeota favoured GDGT-1 to -3 within sediments (Pancost et al., 2001; Blumenberg et al., 2004). MI values spanning 0.3–0.5 indicating a transition between normal marine to a hydrocarbon impacted environments (Zhang et al., 2011). Values > 0.5 indicate the presence of active methanotrophic archaeal communities.

$$\mathrm{MI} = \frac{[\mathrm{GDGT}-1]+[\mathrm{GDGT}-2]+[\mathrm{GDGT}-3]}{[\mathrm{GDGT}-1]+[\mathrm{GDGT}-2]+[\mathrm{GDGT}-3]+[\mathrm{Cren}]+[\mathrm{Cren}']} \quad (18)$$

For the ambient sediments of the Scotian Slope, MI values were consistently low across all sediment depths (Table S9). Ambient sediment IPL-MI ranged from 0.07 to 0.50 (avg. = 0.15) and do not systematically change with depth,

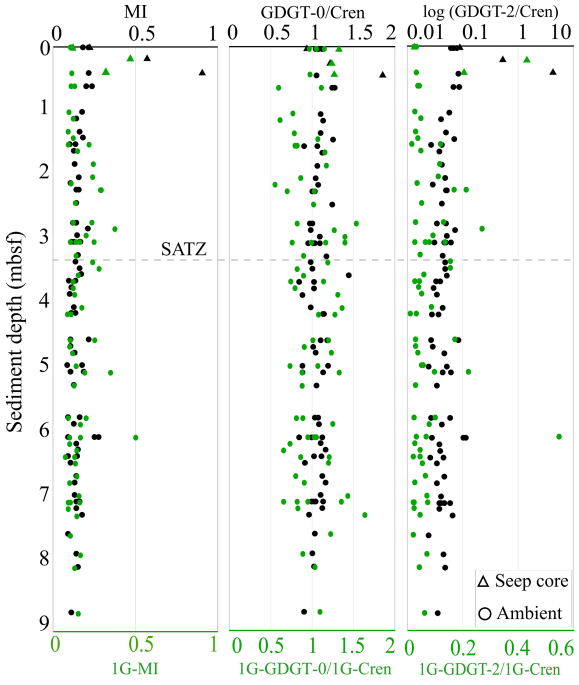

Figure 7. Down core profiles of MI, GDGT-0 / Cren, and GDGT-2 / Cren lipid ratios for CLs (labelled in black) and 1G-IPLs (labelled in green). Dotted line indicates the SATZ.

highlighting a slightly higher proportion of ANME-1 communities within deeper sediments. Core 2018-0007's hydrocarbon seep sediments IPL-MI values range from 0.12 to 0.47; averaged at 0.30 for. Ambient sediment CL-MI have values ranging from 0.08 to 0.27 (avg. = 0.15). Higher CL-MI values are recorded from the seep sediments (ranging from 0.22 to 0.90; avg. = 0.56) suggesting the presence of methanotrophic archaea (Zhang et al., 2011; Fig. 7).

The ratios GDGT-2 / Cren (Zhang et al., 2016) and GDGT-0 / Cren (Blaga et al., 2009) characterize methanogenic archaeal contribution to GDGT pool. GDGT-0 / Cren and GDGT-2 / Cren ratios > 0.2, along with MI > 0.3, indicate methane cycling (Weijers et al., 2011; Zhang et al., 2016; Umoh et al., 2022). For the Scotian Slope, GDGT-0 / Cren ratios were low ranging from 0.84 to 1.86. GDGT-2 / Cren ratios ranged from 0.02 to 4.37 (avg. 0.05 for ambient sediments). Collectively these ratios indicate non-methanogenic contributions to the archaeal pool for the ambient slope sediments. Considerably higher values (avg. 1.34 and 1.67) consistent with active methane cycling (e.g., Teske et al., 2018) were observed within the seep sediments.

With the exception of seep impacted sediments, all biomarker proxies indicate little activity with respect to methane cycling. No systematic changes to ratio values are coupled to any measured porewater geochemical trends (Fig. 2).

4.5 Scotian Slope archaeal lipidomes

4.5.1 Resolution of lipidomes

A heatmap dendrogram of sediment normalized lipid concentrations was calculated to resolve slope-wide diversity patterns (Fig. 8). From this, four distinct groups of lipid classes (labelled as 1a, 1b, 1c, 2, 3, and 4) were resolved. These classes mostly arise from distinct assemblages of IPL, CL, CL-DPs, but also mark differences in water column (i.e., lipid class1a) and sediment (i.e., lipid classes 1b, 1c, 2, and 3) inputs. Additionally, six groups of samples including four main groups and 3 sub-groups (labelled as lipidomes A1, A2, A3, A4.1, A4.2, and A4.3) were further identified representing complex assemblages of living, fossil, and further degraded lipids within the slope sediments.

PCA was performed to further validate the results of the heatmap dendrogram. The results are displayed as both factor loading and score plots with components extracted using eigenvalues greater than one. The first two principal components, accounting for 85 % of the variance in the data, were selected for visualization (Fig. S5). The factor loading plot (Fig. 9) yields three primary lipid clusters (labelled 1–3), with further subdivisions (labelled 1a, 1b, 2, 3a, and 3b). The score plot shows sample clusters that largely group by sediment depth (Fig. 9). Additionally, the scores plot with samples grouped by their location within the four quadrants of the Scotian Slope, as outlined in Fig. 1, indicate no preferential lipidomic changes along the length of the slope (Fig. S6). Collectively, these data largely mirror the patterns observed in the heatmap dendrogram (Fig. 8). The agreement between the two statistical measures suggests specific lipidomic signatures are characteristic features of the deep marine sediments across the Scotian Slope.

4.5.2 Microbial community reconstruction of lipidomes

Although significant limits exist to the extent to which lipid distributions can resolve source organism taxonomy, they nonetheless still mark a quantitative measure of archaeal activity. In this study the resolve Scotian Slope lipidomes indicate systematic vertical change in archaeal microbial communities:

> **Lipidome A1** is dominated by lipid class 2 compounds, including 1G-GDGT-2, GDGT-2, 1G-GDGT-3, GDGT-3, OH-GDGT-1 to -3 as well as 2G-GDGT-0 and AR (Fig. 8), which are commonly produced by methanotrophic archaea and Bathyarchaeia of cold seep environments (Blumenberg et al., 2004; Pancost et al., 2001; Zhang et al., 2011, 2023). A high contribution of ANME-1 in this lipidome is shown by high concentrations of GDGT-2 and GDGT-3, in their IPL and CL forms. Thaumarchaeota group I.1a, is known to produce OH-GDGT compounds under cold, methane-rich conditions (Elling et al., 2017). Lipidome A1 includes sam-

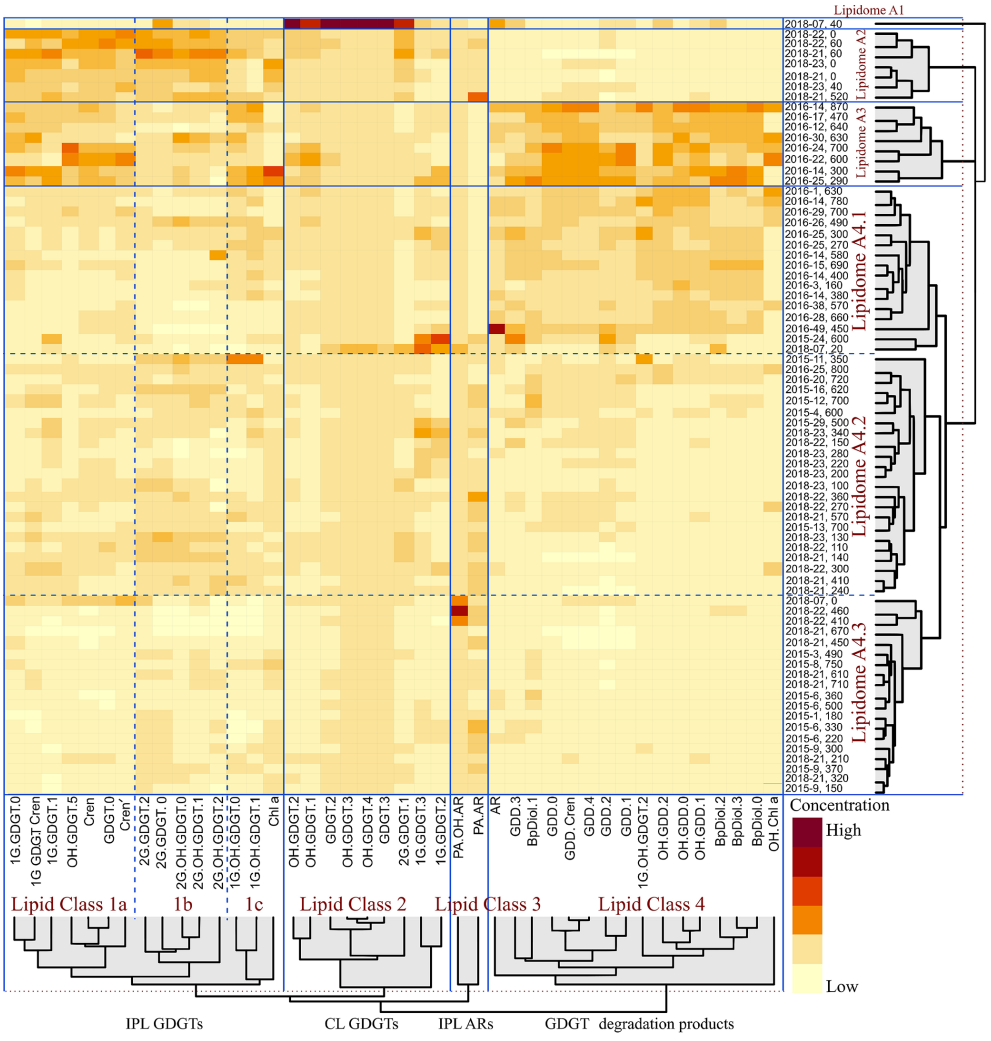

Figure 8. HCA heatmap dendrogram generated displaying the z-scored concentration of archaeal lipid compounds in the 74 sediment samples. Rows mark the individual sediment samples. Columns display normalized z-score concentrations for the different lipid compounds (with the colour gradient indicating elevated concentrations with warmer colours). Red dotted lines indicate the similarity threshold used to distinguish clusters within the HCA dendrogram. Blue dotted lines distinguish sub-groups within clusters.

ples whose core is associated with geochemical and microbial evidence of hydrocarbon seepage (Fowler et al., 2017).

Lipidome A2 is marked by higher concentrations of lipid classes 1a, 1b, and 1c, which includes 1G- and 2G-GDGTs, as well as GDGT-0, Cren, and Cren' that are known to be mainly synthesized by non-thermophilic ammonia-oxidizing Thaumarchaeota inhabiting surface and shallow sediments (Schouten et al., 2000, 2002, 2013). A strong contribution from non-thermophilic Thaumarchaeota, particularly Thaumarchaeota group I.1a in lipidome A2 is supported by high concentrations of Cren and GDGT-0 (Schouten et al., 2000, 2002, 2013).

Lipidomes A3 and A4s are dominated by compounds from lipid class 4 that have higher contributions of GDGT degradation products such as GDDs, OH-GDDs, and Bp-Diols. Additionally, high concentration of Cren and GDGT-0 supports a strong contribution from non-thermophilic Thaumarchaeota in this lipidome (Schouten et al., 2000, 2002, 2013). High AR and CL-DPs concentration in lipidomes A3 and A4.1 indicates increased contribution of methanogens and ANME groups (Pancost et al., 2011; Rossel et al., 2008) as well as methanogenic archaea (Liu et al., 2012b; Meador et al., 2014; Bauersachs et al., 2015). Lipidomes A4.2 and A4.3 exhibit the lowest concentrations of archaeal lipids including GDGT degradation products (lipid class 4). These lipidomes are likely dominated by Thaumarchaeota, particularly

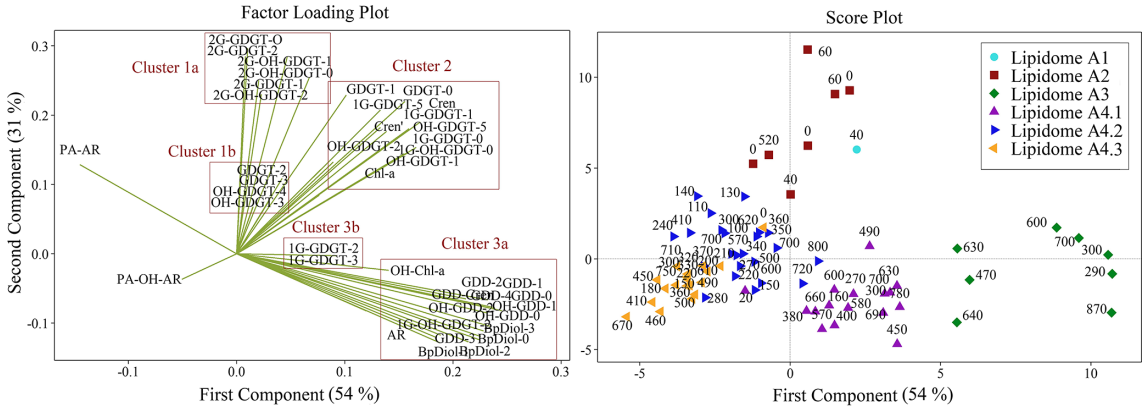

Figure 9. Principal component analysis of archaeal lipid concentrations. Factor loadings plot (left) displaying five distinct clusters. Within the score plot (right), sediment samples are grouped corresponding to the six lipidomes (numerical labels indicate the sediment burial depth of each sample in centimetres).

non-thermophilic groups such as Thaumarchaeota I.1a, which produce IPLs and core GDGTs (Elling et al., 2017).

Only one of the four stratigraphically controlled lipidomes (A1 from a prospective cold seep) is detectable by the surveyed environmental biomarker proxies (Fig. 7). This indicates biomarker proxies may not resolve some complex changes to archaeal community structures within marine sedimentary systems. Additionally, individual lipidomes do not typically produce correlated lipid pairs of diagenetic alteration steps (Sect. 4.4; Fig. 5).

4.6 Controlling factors and the spatial extent of the Scotian Slope lipostratigraphy

The six lipidomes have overlapping sediment depth ranges (Fig. 10). The spatial extent of each lipidome was interpolated from the outermost perimeter of depth equivalent core locations from which it could be resolved (Fig. 11) to reveal a slope wide archaeal lipostrigraphy. The mechanism for how these zones formed is unclear. One potential driver is sedimentology. Lithology affects porewater permeability, pH, and nutrient loading, which in turn could impact the archaeal community structure. To test this, sedimentological observations taken from cruise core logs (Table S2) were used to examine lipidomic linkages to lithology by statically comparing texture (suggestive of grain size changes), colour (corresponding to mineralogy and potentially redox changes), and sedimentary structures to lipidome occurrences (Fig. S7). These analyses did not produce meaningful statistical relationships. As such, sediment lithology (Fig. S7), changes in organic matter loading (Fig. 2), methane cycling (Fig. 7) and latitudinal position along the outlined slope quadrants (Figs. 1 and S6) do not fundamentally impact the archaeal lipostratigraphy (Fig. 11). Alternatively, microbial redox-controlled biogeochemical cycles are well defined within marine sedimentary systems. Slope-wide geochemical porewater profiles of sulfate and DIC (Figs. 2 and 10) indicate a complimentary occurrence of elevated microbial sulfate reduction. Lipidomes 3 and 4 occur near the sulphate alkalinity transition zone at $\sim$3.25 m b.s.f. (Fig. 10). This depth coincides with the beginning of the lipidomes A3 and A4.1. In this regard, sediment accumulation coupled to diffusion limitation appears to be driving stratified redox controlled biogeochemical zones that are mediated and affected by partially niche-partitioned microbial habitats. Additionally, burial depth was shown to affect lipid preservation (Figs. 5 and 6).

5 Conclusions

This study quantified archaeal lipid classes from sediment collected along the Scotian Slope of Northeastern Atlantic, Canada. The survey extended to $\sim$9 m below the ocean floor and spanned $\sim$40 000 km^2, traversing $\sim$3° of latitudinal change, with an overlying water column that increased from $\sim$1500 to 3500 m depth. Archaeal lipids were found to be sourced from both the water column and ocean floor sediments. Measured diagenetic decay rates indicate the chemical structure of a lipid impacts its preservation with typically higher CL-DP and CL rates arising relative to that of IPLs. Additionally, lipid diversity and abundance systematically vary with sediment depth forming four stratigraphically overlapping lipidomes with high ANME-1 contributions. One of these represents contributions from an archaeal community impacted by an isolated seep environment. The other three, mark ambient sediment lipidomes that reflect $\sim 27 \pm 4$ Kyr of changing water column loading, mixed with in situ sedimentary additions from subsurface archaeal communities. These lipidomes are further augmented by increasing abundances of archaeal lipid degradation products. The ambient sediment lipidomes appear highly conserved across the latitudinal ex-

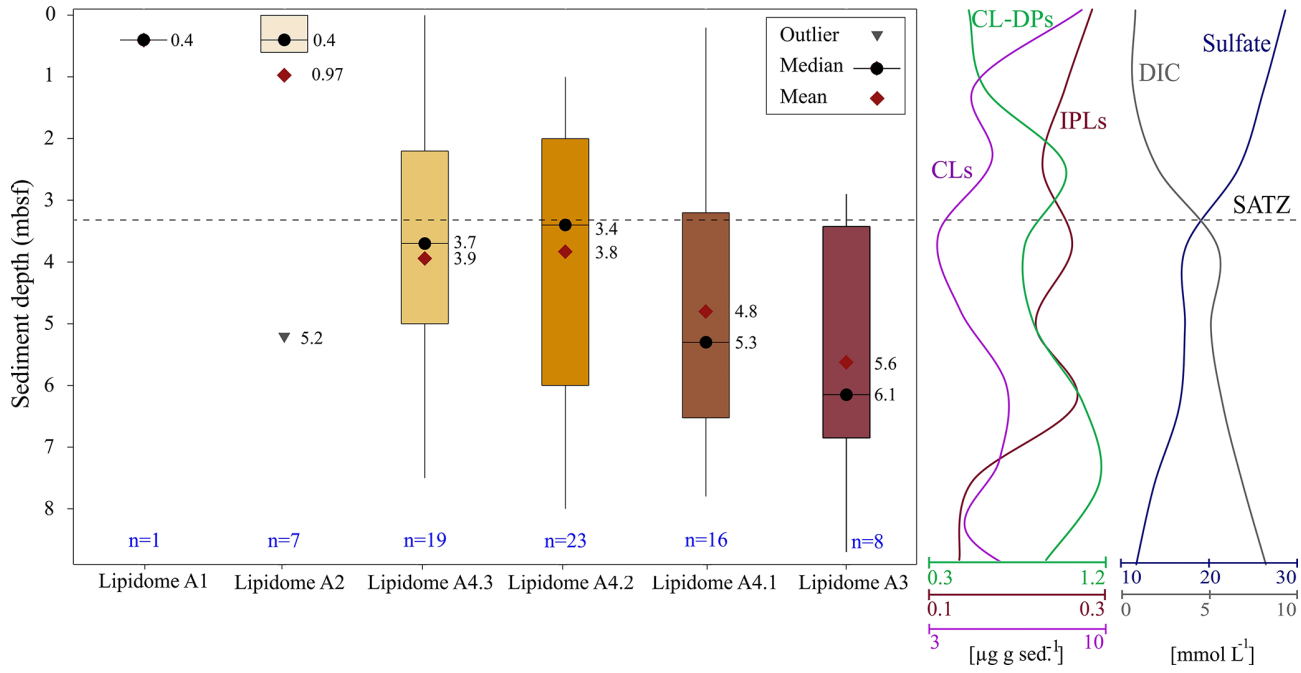

Figure 10. Box-and-whisker plot displaying the interquartile sediment burial depth ranges of the six heatmap dendrogram resolved lipidomes (Fig. 8), along with the smoothed down core profile showing the slope averaged concentration of IPLs, CLs, CL-DPs, sulfate, and DIC made using the average concentration at 1 m depth intervals (Fig. 2). The SATZ is labelled at the cross-over of the two down core profiles. The number of sediment samples contributing to each lipidome in the box plot is reported in blue font. The values for outlier, mean, and median refers to one meter core depths.

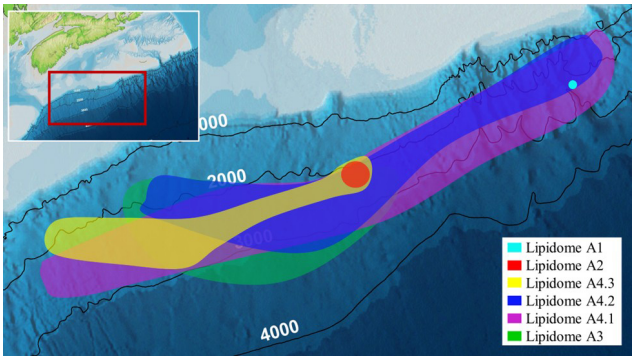

Figure 11. Scotian Slope bathymetric map showing the spatial extent of the archaeal lipostratigraphy.

tent of the study area marking a resolvable shallow sediment lipostratigraphy for the Scotian Slope.

Data availability. Relevant data sets are provided in the Supplement for this publication.

Supplement. The supplement related to this article is available online at https://doi.org/10.5194/bg-23-21-2026-supplement.

Author contributions. NA and GTV designed the research and wrote the manuscript. NA generated the lipid data and provided the data analysis. UU provided technical support with lipid identification. NM provided geographical data. AM provided logistical support for sampling and project completion. ER and PG provided analytical support with bulk geochemistry and molecular analyses. MGF provided technical support for the interpretation of site localities. JNB provided technical support and helped to collect samples. VB provided technical support for porewater analysis.

Competing interests. The contact author has declared that none of the authors has any competing interests.

Disclaimer. Publisher's note: Copernicus Publications remains neutral with regard to jurisdictional claims made in the text, published maps, institutional affiliations, or any other geographical representation in this paper. While Copernicus Publications makes every effort to include appropriate place names, the final responsibility lies with the authors. Views expressed in the text are those of the authors and do not necessarily reflect the views of the publisher.

Acknowledgements. Thanks to the Nova Scotia Provincial Government for support of this project and spear-heading the various research cruises and surveys that made the integrative data collection possible. A special thanks is given to Carey Ryan of Net Zero At-

lantic, who was the GAPP Partnership Program manager responsible for the larger group research initiatives. Carey also managed the procuration and organization of the research cruises. We would also like to acknowledge that Julius Lipp, Florence Schubotz, and Kai-Uwe Hinrichs of MARUM, University of Bremen were instrumental in helping to first develop SMU's techniques in lipidomics. An additional special thanks is given to Kim Doane, the executive director of the Subsurface and Offshore Energy Branch of the Department of Energy for her support of the Organic Geochemistry Research Group at Saint Mary's University. Sediment samples analysed in this study were collected during three marine field programs led by the Geological Survey of Canada under a joint collaborative research agreement with Nova Scotian Department of Natural Resources and Renewables. Kate Jarrett of Natural Resources Canada provided the core logs that were used to describe the sediment lithologies used for the study. Nikita Lakhanpal provided porewater analyses for this study. We would like to extend special thanks to Associate editor Sebastian Naeher and the reviewers of this paper for the efforts in improving the quality and clarity of the study.

Financial support. Funding for this project was sourced from: Genome Atlantic and Genome Canada; Research Nova Scotia (grant no. 2142); Mitacs (grant nos. IT12481 and IT29547), NetZero Atlantic and the Nova Scotia This research has been supported by the Natural Sciences and Engineering Research Council of Canada (grant no. RGPIN-2018-06147; NSERC), NSERC Canada Research Chairs (CRC) program, Canada Foundation for Innovation (CFI; JELF–CRC, John R. Evans Leaders Fund), NSERC Discovery Grants program (application no. RGPIN-2017-05822).

Review statement. This paper was edited by Sebastian Naeher and reviewed by Ronnakrit Rattanasriampaipong and three anonymous referees.

References

Arndt, S., Jørgensen, B. B., LaRowe, D. E., Middelburg, J. J., Pancost, R. D., and Regnier, P.: Quantifying the degradation of organic matter in marine sediments: A review and synthesis, Earth-Sci. Rev., 123, 53–86, https://doi.org/10.1016/j.earscirev.2013.02.008, 2013.

Bauersachs, T., Weidenbach, K., Schmitz, R. A., and Schwark, L.: Distribution of glycerol ether lipids in halophilic, methanogenic and hyperthermophilic archaea, Org. Geochem., 83–84, 101–108, https://doi.org/10.1016/j.orggeochem.2015.03.009, 2015.

Bennett, R. and Desiage, P.-A.: Expedition report 21CONDOR: Scotian Slope, 14–29 August 2021 (Open File 8889, Geological Survey of Canada, 2022), https://doi.org/10.4095/329977, 2022.

Bentley, J. N., Ventura, G. T., Walters, C. C., Sievert, S. M., and Seewald, J. S.: The influence of near-surface sediment hydrothermalism on the TEX86 tetraether-lipid-based proxy and a new correction for ocean bottom lipid overprinting, Biogeosciences, 19, 4459–4477, https://doi.org/10.5194/bg-19-4459-2022, 2022.

Berner, R. A.: Early Diagenesis: A theoretical Approach. Princeton University Press, Princeton, 241 pp., ISBN 9780691082608, 1980.

Biddle, J. F., Lipp, J. S., Lever, M. A., Lloyd, K. G., Sørensen, K. B., Anderson, R., Fredricks, H. F., Elvert, M., Kelly, T. J., Schrag, D. P., Sogin, M. L., Brenchley, J. E., Teske, A., House, C. H., and Hinrichs, K.-U.: Heterotrophic Archaea dominate sedimentary subsurface ecosystems off Peru, Proc. Natl. Acad. Sci. U.S.A., 103, 3846–3851, https://doi.org/10.1073/pnas.0600035103, 2006.

Blaga, C. I., Reichart, G.-J., Heiri, O., and Sinninghe Damsté, J. S.: Tetraether membrane lipid distributions in water-column particulate matter and sediments: a study of 47 European lakes along a north–south transect, J. Paleolimnol., 41, 523–540, https://doi.org/10.1007/s10933-008-9242-2, 2009.

Bligh, E. G. and Dyer, W. J.: A Rapid Method of Total Lipid Extraction and Purification, Can. J. Biochem. Physiol., 37, 911–917, 1959.

Blumenberg, M., Seifert, R., Reitner, J., Pape, T., and Michaelis, W.: Membrane lipid patterns typify distinct anaerobic methanotrophic consortia, Proc. Natl. Acad. Sci. U.S.A., 101, 11111–11116, https://doi.org/10.1073/pnas.0401188101, 2004.

Boetius, A., Ravenschlag, K., Schubert, C. J., Rickert, D., Widdel, F., Gieseke, A., Amann, R., Jørgensen, B. B., Witte, U., and Pfannkuche, O.: A marine microbial consortium apparently mediating anaerobic oxidation of methane, Nature, 407, 623–626, https://doi.org/10.1038/35036572, 2000.

Burdige, D. J.: Preservation of Organic Matter in Marine Sediments: Controls, Mechanisms, and an Imbalance in Sediment Organic Carbon Budgets?, Chem. Rev., 107, 467–485, https://doi.org/10.1021/cr050347q, 2007.

Campbell, D. C.: CCGS Hudson Expedition 2016-011, phase 2. Cold seep investigations on the Scotian Slope, offshore Nova Scotia, 15 June–6 July 2016 (Geological Survey of Canada, Open File, 8525), https://doi.org/10.4095/313603, 2019.

Campbell, D. C. and MacDonald, A. W. A.: CCGS Hudson Expedition 2015-018, geological investigation of potential seabed seeps along the Scotian Slope, 25 June–9 July 2015 (Geological Survey of Canada, Open File, 8116), https://doi.org/10.4095/299390, 2016.

Campbell, D. C. and Normandeau, A.: CCGS Hudson Expedition 2018-041: high-resolution investigation of deep-water seabed seeps and landslides along the Scotian Slope, offshore Nova Scotia, May 26–June 15, 2018 (Geological Survey of Canada, Open File, 8567), https://doi.org/10.4095/314695, 2019.

Carr, S. A., Schubotz, F., Dunbar, R. B., Mills, C. T., Dias, R., Summons, R. E., and Mandernack, K. W.: Acetoclastic Methanosaeta are dominant methanogens in organic-rich Antarctic marine sediments, The ISME Journal, 12, 330–342, https://doi.org/10.1038/ismej.2017.150, 2018.

Cheng, Z., Yu, F., Ruan, X., Cheng, P., Chen, N., Tao, S., Zong, Y., Yang, H., and Huang, Z.: GDGTs as indicators for organic-matter sources in a small subtropical river-estuary system, Org. Geochem., 153, 104180, https://doi.org/10.1016/j.orggeochem.2021.104180, 2021.

Chowdhury, A., Ventura, G. T., Owino, Y., Lalk, E. J., MacAdam, N., Dooma, J. M., Ono, S., Fowler, M., MacDonald, A., Bennett, R., MacRae, R. A., Hubert, C. R. J., Bentley, J. N., and Kerr, M. J.: Cold seep formation from salt diapir–controlled deep biosphere oases, Proc. Natl. Acad. Sci. U.S.A., 121, e2316878121, https://doi.org/10.1073/pnas.2316878121, 2024.

Coffinet, S., Huguet, A., Williamson, D., Bergonzini, L., Anquetil, C., Majule, A., and Derenne, S.: Occurrence and distribution of glycerol dialkanol diethers and glycerol dialkyl glycerol tetraethers in a peat core from SW Tanzania, Organic Geochemistry, 83–84, 170–177, https://doi.org/10.1016/j.orggeochem.2015.03.013, 2015.

De Rosa, M.: Archaeal lipids: structural features and supramolecular organization, Thin Solid Films, 284–285, 13–17, https://doi.org/10.1016/S0040-6090(96)08832-3, 1996.

Dong, X., Rattray, J. E., Campbell, D. C., Webb, J., Chakraborty, A., Adebayo, O., Matthews, S., Li, C., Fowler, M., Morrison, N. M., MacDonald, A., Groves, R. A., Lewis, I. A., Wang, S. H., Mayumi, D., Greening, C., and Hubert, C. R. J.: Thermogenic hydrocarbon biodegradation by diverse depth-stratified microbial populations at a Scotian Basin cold seep, Nat. Commun., 11, 5825, https://doi.org/10.1038/s41467-020-19648-2, 2020.

Elling, F. J., Könneke, M., Nicol, G. W., Stieglmeier, M., Bayer, B., Spieck, E., De La Torre, J. R., Becker, K. W., Thomm, M., Prosser, J. I., Herndl, G. J., Schleper, C., and Hinrichs, K.: Chemotaxonomic characterisation of the thaumarchaeal lipidome, Environ. Microbiol., 19, 2681–2700, https://doi.org/10.1111/1462-2920.13759, 2017.

Evans, T. W., Wörmer, L., Lever, M. A., Lipp, J. S., Lagostina, L., Lin, Y.-S., Jørgensen, B. B., and Hinrichs, K.-U.: Size and composition of subseafloor microbial community in the Benguela upwelling area examined from intact membrane lipid and DNA analysis, Org. Geochem., 111, 86–100, https://doi.org/10.1016/j.orggeochem.2017.06.008, 2017.

Fowler, M., Webb, J., Olsen, H., Ashraf, F., and Guldbrandsen, S.: Geochemistry data report for 2016 Scotian Slope piston coring program, https://oera.ca/research/piston-coring-geochemistry-program (last access: 2018), 2017.

Fredricks, H. F. and Hinrichs, K.-U.: Proceedings of the Ocean Drilling Program, 207 Scientific Results, Ocean Drilling Program, https://doi.org/10.2973/odp.proc.sr.207.2007, 2007.

Gittins, D. A., Desiage, P.-A., Morrison, N., Rattray, J. E., Bhatnagar, S., Chakraborty, A., Zorz, J., Li, C., Horanszky, O., Cramm, M. A., Bisiach, F., Bennett, R., Webb, J., MacDonald, A., Fowler, M., Campbell, D. C., and Hubert, C. R. J.: Geological processes mediate a microbial dispersal loop in the deep biosphere, Sci. Adv., 8, eabn3485, https://doi.org/10.1126/sciadv.abn3485, 2022.

Guan, H., Feng, D., Wu, N., and Chen, D.: Methane seepage intensities traced by biomarker patterns in authigenic carbonates from the South China Sea, Org. Geochem., 91, 109–119, https://doi.org/10.1016/j.orggeochem.2015.11.007, 2016.

Guo, W., Xie, W., Li, X., Wang, P., Hu, A., and Zhang, C. L.: Environmental factors shaping the archaeal community structure and ether lipid distribution in a subtropic river and estuary, China, Appl. Microbiol. Biotechnol., 102, 461–474, https://doi.org/10.1007/s00253-017-8595-8, 2018.

Hingley, J. S., Martins, C. C., Walker-Trivett, C., Adams, J. K., Naeher, S., Häggi, C., Feakins, S. J., and Naafs, B. D. A.: The global distribution of Isoprenoidal Glycerol Dialkyl Diethers (isoGDDs) is consistent with a predominant degradation origin, Org. Geochem., 192, 104782, https://doi.org/10.1016/j.orggeochem.2024.104782, 2024.

Hinrichs, K.-U., Summons, R. E., Orphan, V., Sylva, S. P., and Hayes, J. M.: Molecular and isotopic analysis of anaerobic methane-oxidizing communities in marine sediments, Org. Geochem., 31, 1685–1701, https://doi.org/10.1016/S0146-6380(00)00106-6, 2000.

Hoshino, T., Doi, H., Uramoto, G.-I., Wörmer, L., Adhikari, R. R., Xiao, N., Morono, Y., D'Hondt, S., Hinrichs, K.-U., and Inagaki, F.: Global diversity of microbial communities in marine sediment, Proc. Natl. Acad. Sci. U.S.A., 117, 27587–27597, https://doi.org/10.1073/pnas.1919139117, 2020.

Hu, A., Hou, L., and Yu, C.-P.: Biogeography of Planktonic and Benthic Archaeal Communities in a Subtropical Eutrophic Estuary of China, Microb. Ecol., 70, 322–335, https://doi.org/10.1007/s00248-015-0597-4, 2015.

Hurley, S. J., Elling, F. J., Könneke, M., Buchwald, C., Wankel, S. D., Santoro, A. E., Lipp, J. S., Hinrichs, K.-U., and Pearson, A.: Influence of ammonia oxidation rate on thaumarchaeal lipid composition and the TEX_{86} temperature proxy, Proc. Natl. Acad. Sci. U.S.A., 113, 7762–7767, https://doi.org/10.1073/pnas.1518534113, 2016.

Ingalls, A. E., Huguet, C., and Truxal, L. T.: Distribution of Intact and Core Membrane Lipids of Archaeal Glycerol Dialkyl Glycerol Tetraethers among Size-Fractionated Particulate Organic Matter in Hood Canal, Puget Sound, Appl. Environ. Microbiol., 78, 1480–1490, https://doi.org/10.1128/AEM.07016-11, 2012.

Jenner, K. A., Campbell, D. C., Barnett, J. M., Higgins, J., and Normandeau, A.: Piston cores and supporting high-resolution seismic data, CCGS Hudson Expedition 2015018, Scotian Slope, offshore Nova Scotia, Canada, https://doi.org/10.4095/330088, 2022.

Kim, J.-H., Van Der Meer, J., Schouten, S., Helmke, P., Willmott, V., Sangiorgi, F., Koç, N., Hopmans, E. C., and Damsté, J. S. S.: New indices and calibrations derived from the distribution of crenarchaeal isoprenoid tetraether lipids: Implications for past sea surface temperature reconstructions, Geochim. Cosmochim. Acta, 74, 4639–4654, https://doi.org/10.1016/j.gca.2010.05.027, 2010.

Knappy, C. S. and Keely, B. J.: Novel glycerol dialkanol triols in sediments: transformation products of glycerol dibiphytanyl glycerol tetraether lipids or biosynthetic intermediates?, Chem. Commun., 48, 841–843, https://doi.org/10.1039/C1CC15841D, 2012.

Knittel, K. and Boetius, A.: Anaerobic Oxidation of Methane: Progress with an Unknown Process, Annu. Rev. Microbiol., 63, 311–334, https://doi.org/10.1146/annurev.micro.61.080706.093130, 2009.

Koelmel, J. P., Napolitano, M. P., Ulmer, C. Z., Vasiliou, V., Garrett, T. J., Yost, R. A., Prasad, M. N. V., Godri Pollitt, K. J., and Bowden, J. A.: Environmental lipidomics: understanding the response of organisms and ecosystems to a changing world, Metabolomics, 16, 56, https://doi.org/10.1007/s11306-020-01665-3, 2020.

Koga, Y., Nishihara, M., Morii, H., and Akagawa-Matsushita, M.: Ether Polar Lipids of Methanogenic Bacteria: Structures, Comparative Aspects, and Biosyntheses, Microbiol. Rev., 57, https://doi.org/10.1128/mr.57.1.164-182.1993, 1993.

Lengger, S. K., Kraaij, M., Tjallingii, R., Baas, M., Stuut, J.-B., Hopmans, E. C., Sinninghe Damsté, J. S., and Schouten, S.: Differential degradation of intact polar and core glycerol dialkyl glycerol tetraether lipids upon

post-depositional oxidation, Org. Geochem., 65, 83–93, https://doi.org/10.1016/j.orggeochem.2013.10.004, 2013.

Lengger, S. K., Lipsewers, Y. A., de Haas, H., Sinninghe Damsté, J. S., and Schouten, S.: Lack of ^{13}C-label incorporation suggests low turnover rates of thaumarchaeal intact polar tetraether lipids in sediments from the Iceland shelf, Biogeosciences, 11, 201–216, https://doi.org/10.5194/bg-11-201-2014, 2014.

Li, C., Adebayo, O., Ferguson, D. K., Wang, S., Rattray, J. E., Fowler, M., Webb, J., Campbell, C., Morrison, N., MacDonald, A., and Hubert, C. R. J.: Bacterial anomalies associated with deep sea hydrocarbon seepage along the Scotian Slope, Deep-Sea Res. I: Oceanogr. Res. Pap., 193, 103955, https://doi.org/10.1016/j.dsr.2022.103955, 2023.

Li, J., Pancost, R. D., Naafs, B. D. A., Yang, H., Zhao, C., and Xie, S.: Distribution of glycerol dialkyl glycerol tetraether (GDGT) lipids in a hypersaline lake system, Org. Geochem., 99, 113–124, https://doi.org/10.1016/j.orggeochem.2016.06.007, 2016.

Lin, Y., Lipp, J. S., Elvert, M., Holler, T., and Hinrichs, K.: Assessing production of the ubiquitous archaeal diglycosyl tetraether lipids in marine subsurface sediment using intramolecular stable isotope probing, Environ. Microbiol., 15, 1634–1646, https://doi.org/10.1111/j.1462-2920.2012.02888.x, 2013.

Lipp, J. S. and Hinrichs, K.-U.: Structural diversity and fate of intact polar lipids in marine sediments, Geochim. Cosmochim. Acta, 73, 6816–6833, https://doi.org/10.1016/j.gca.2009.08.003, 2009.

Lipp, J. S., Morono, Y., Inagaki, F., and Hinrichs, K.-U.: Significant contribution of Archaea to extant biomass in marine subsurface sediments, Nature, 454, 991–994, https://doi.org/10.1038/nature07174, 2008.

Liu, X., Summons, R. E., and Hinrichs, K.: Extending the known range of glycerol ether lipids in the environment: structural assignments based on tandem mass spectral fragmentation patterns, Rap. Comm. Mass Spectrom., 26, 2295–2302, https://doi.org/10.1002/rcm.6355, 2012a.

Liu, X.-L., Lipp, J. S., Schröder, J. M., Summons, R. E., and Hinrichs, K.-U.: Isoprenoid glycerol dialkanol diethers: A series of novel archaeal lipids in marine sediments, Org. Geochem., 43, 50–55, https://doi.org/10.1016/j.orggeochem.2011.11.002, 2012b.

Liu, X.-L., Lipp, J. S., Simpson, J. H., Lin, Y.-S., Summons, R. E., and Hinrichs, K.-U.: Mono- and dihydroxyl glycerol dibiphytanyl glycerol tetraethers in marine sediments: Identification of both core and intact polar lipid forms, Geochim. Cosmochim. Acta, 89, 102–115, https://doi.org/10.1016/j.gca.2012.04.053, 2012c.

Liu, X.-L., Birgel, D., Elling, F. J., Sutton, P. A., Lipp, J. S., Zhu, R., Zhang, C., Könneke, M., Peckmann, J., Rowland, S. J., Summons, R. E., and Hinrichs, K.-U.: From ether to acid: A plausible degradation pathway of glycerol dialkyl glycerol tetraethers, Geochim. Cosmochim. Acta, 183, 138–152, https://doi.org/10.1016/j.gca.2016.04.016, 2016.

Liu, X.-L., Lipp, J. S., Birgel, D., Summons, R. E., and Hinrichs, K.-U.: Predominance of parallel glycerol arrangement in archaeal tetraethers from marine sediments: Structural features revealed from degradation products, Org. Geochem., 115, 12–23, https://doi.org/10.1016/j.orggeochem.2017.09.009, 2018.

Meador, T. B., Zhu, C., Elling, F. J., Könneke, M., and Hinrichs, K.-U.: Identification of isoprenoid glycosidic glycerol dibiphytanol diethers and indications for their biosynthetic origin, Org. Geochem., 69, 70–75, https://doi.org/10.1016/j.orggeochem.2014.02.005, 2014.

Middelburg, J. J.: Marine Carbon Biogeochemistry: A Primer for Earth System Scientists, Springer International Publishing, Cham, https://doi.org/10.1007/978-3-030-10822-9, 2019.

Mitrović, D., Hopmans, E. C., Bale, N. J., Richter, N., Amaral-Zettler, L. A., Baxter, A. J., Peterse, F., Miguel Raposeiro, P., Gonçalves, V., Cristina Costa, A., and Schouten, S.: Isoprenoidal GDGTs and GDDs associated with anoxic lacustrine environments, Org. Geochem., 178, 104582, https://doi.org/10.1016/j.orggeochem.2023.104582, 2023.

Offre, P., Spang, A., and Schleper, C.: Archaea in Biogeochemical Cycles, Annu. Rev. Microbiol., 67, 437–457, https://doi.org/10.1146/annurev-micro-092412-155614, 2013.

Orcutt, B. N., Sylvan, J. B., Knab, N. J., and Edwards, K. J.: Microbial Ecology of the Dark Ocean above, at, and below the Seafloor, Microbiol. Mol. Biol. Rev., 75, 361–422, https://doi.org/10.1128/MMBR.00039-10, 2011.

Pancost, R. D., Hopmans, E. C., and Sinninghe Damsté, J. S.: Archaeal lipids in Mediterranean cold seeps: molecular proxies for anaerobic methane oxidation, Geochim. Cosmochim. Acta, 65, 1611–1627, https://doi.org/10.1016/S0016-7037(00)00562-7, 2001.

Pancost, R. D., McClymont, E. L., Bingham, E. M., Roberts, Z., Charman, D. J., Hornibrook, E. R. C., Blundell, A., Chambers, F. M., Lim, K. L. H., and Evershed, R. P.: Archaeol as a methanogen biomarker in ombrotrophic bogs, Org. Geochem., 42, 1279–1287, https://doi.org/10.1016/j.orggeochem.2011.07.003, 2011.

Rattray, J. E., Elizondo, G., Sloan, K., Morrison, N., Fowler, M., Gittins, D. A., Webb, J., Calvin Campbell, D., MacDonald, A., and Hubert, C. R. J.: Elevated bacterial endospores associated with thermogenic hydrocarbon seeps in deep sea sediments, Org. Geochem., 177, 104568, https://doi.org/10.1016/j.orggeochem.2023.104568, 2023.

Rinke, C., Chuvochina, M., Mussig, A. J., Chauneil, P.-A., Waite, D. W., Whitman, W. B., Parks, D. H., and Hugenholtz, P.: A standardized archaeal taxonomy for the Genome Taxonomy Database, Nat. Microbiol., 6, 946–959, https://doi.org/10.1038/s41564-021-00918-8, 2021.

Rossel, P. E., Lipp, J. S., Fredricks, H. F., Arnds, J., Boetius, A., Elvert, M., and Hinrichs, K.-U.: Intact polar lipids of anaerobic methanotrophic archaea and associated bacteria, Org. Geochem., 39, 992–999, https://doi.org/10.1016/j.orggeochem.2008.02.021, 2008.

Rossel, P. E., Elvert, M., Ramette, A., Boetius, A., and Hinrichs, K.-U.: Factors controlling the distribution of anaerobic methanotrophic communities in marine environments: Evidence from intact polar membrane lipids, Geochim. Cosmochim. Acta, 75, 164–184, https://doi.org/10.1016/j.gca.2010.09.031, 2011.

Schouten, S., Hopmans, E. C., Pancost, R. D., and Damsté, J. S. S.: Widespread occurrence of structurally diverse tetraether membrane lipids: Evidence for the ubiquitous presence of low-temperature relatives of hyperthermophiles, Proc. Natl. Acad. Sci. U.S.A., 97, 14421–14426, https://doi.org/10.1073/pnas.97.26.14421, 2000.

Schouten, S., Hopmans, E. C., Schefuß, E., and Sinninghe Damsté, J. S.: Distributional variations in marine crenarchaeotal membrane lipids: a new tool for reconstructing ancient sea wa-

ter temperatures?, Earth. Planet. Sci. Lett., 204, 265–274, https://doi.org/10.1016/S0012-821X(02)00979-2, 2002.

Schouten, S., Baas, M., Hopmans, E. C., and Sinninghe Damsté, J. S.: An unusual isoprenoid tetraether lipid in marine and lacustrine sediments, Org. Geochem., 39, 1033–1038, https://doi.org/10.1016/j.orggeochem.2008.01.019, 2008.

Schouten, S., Middelburg, J. J., Hopmans, E. C., and Sinninghe Damsté, J. S.: Fossilization and degradation of intact polar lipids in deep subsurface sediments: A theoretical approach, Geochim. Cosmochim. Acta, 74, 3806–3814, https://doi.org/10.1016/j.gca.2010.03.029, 2010.

Schouten, S., Hopmans, E. C., and Sinninghe Damsté, J. S.: The organic geochemistry of glycerol dialkyl glycerol tetraether lipids: A review, Org. Geochem., 54, 19–61, https://doi.org/10.1016/j.orggeochem.2012.09.006, 2013.

Schubotz, F., Wakeham, S. G., Lipp, J. S., Fredricks, H. F., and Hinrichs, K.: Detection of microbial biomass by intact polar membrane lipid analysis in the water column and surface sediments of the Black Sea, Environ. Microbiol., 11, 2720–2734, https://doi.org/10.1111/j.1462-2920.2009.01999.x, 2009.

Schubotz, F., Lipp, J. S., Elvert, M., and Hinrichs, K.-U.: Stable carbon isotopic compositions of intact polar lipids reveal complex carbon flow patterns among hydrocarbon degrading microbial communities at the Chapopote asphalt volcano, Geochim. Cosmochim. Acta, 75, 4399–4415, https://doi.org/10.1016/j.gca.2011.05.018, 2011.

Sinninghe Damsté, J. S., Rijpstra, W. I. C., Hopmans, E. C., Den Uijl, M. J., Weijers, J. W. H., and Schouten, S.: The enigmatic structure of the crenarchaeol isomer, Org. Geochem., 124, 22–28, https://doi.org/10.1016/j.orggeochem.2018.06.005, 2018.

Sollich, M., Yoshinaga, M. Y., Häusler, S., Price, R. E., Hinrichs, K.-U., and Bühring, S. I.: Heat Stress Dictates Microbial Lipid Composition along a Thermal Gradient in Marine Sediments, Front. Microbiol., 8, 1550, https://doi.org/10.3389/fmicb.2017.01550, 2017.

Sturt, H. F., Summons, R. E., Smith, K., Elvert, M., and Hinrichs, K.: Intact polar membrane lipids in prokaryotes and sediments deciphered by high-performance liquid chromatography/electrospray ionization multistage mass spectrometry – new biomarkers for biogeochemistry and microbial ecology, Rap. Comm. Mass Spectrom., 18, 617–628, https://doi.org/10.1002/rcm.1378, 2004.

Teske, A., Lizarralde, D., and Höfig, T. W.: Expedition 385 Scientific Prospectus: Guaymas Basin Tectonics and Biosphere: feedbacks between continental rifting, magmatism, sedimentation, thermal alteration of organic matter, and microbial activity, Int. Ocean Dis. Prog., https://doi.org/10.14379/iodp.sp.385.2018, 2018.

Umoh, U. U., Li, L., Wang, J., Kauluma, N., Asuquo, F. E., and Akpan, E. R.: Glycerol dialkyl glycerol tetraether signatures in tropical mesotidal estuary sediments of Qua Iboe River, Gulf of Guinea, Org. Geochem., 170, 104461, https://doi.org/10.1016/j.orggeochem.2022.104461, 2022.

Valentine, D. L.: Adaptations to energy stress dictate the ecology and evolution of the Archaea, Nat. Rev. Microbiol., 5, 316–323, https://doi.org/10.1038/nrmicro1619, 2007.

Villanueva, L., Damsté, J. S. S., and Schouten, S.: A re-evaluation of the archaeal membrane lipid biosynthetic pathway, Nat. Rev. Microbiol., 12, 438–448, https://doi.org/10.1038/nrmicro3260, 2014.

Wade, J. A. and MacLean, B. C.: The geology of the Southeastern Margin of Canada, Chapter 5, in: Geology of the Continental Margin of Eastern Canada, edited by: Keen, M. J. and Williams, G. L., Geological Survey of Canada, The Geology of Canada, 190–238, https://doi.org/10.1130/DNAG-GNA-I1.167, 1990.

Wallmann, K., Aloisi, G., Haeckel, M., Obzhirov, A., Pavlova, G., and Tishchenko, P.: Kinetics of organic matter degradation, microbial methane generation, and gas hydrate formation in anoxic marine sediments, Geochim. Cosmochim. Acta, 70, 3905–3927, https://doi.org/10.1016/j.gca.2006.06.003, 2006.

Weijers, J. W. H., Lim, K. L. H., Aquilina, A., Sinninghe Damsté, J. S., and Pancost, R. D.: Biogeochemical controls on glycerol dialkyl glycerol tetraether lipid distributions in sediments characterized by diffusive methane flux: TEX_{86} in Sulfate - Methane Transition Zone, Geochem. Geophys. Geosyst., 12, https://doi.org/10.1029/2011GC003724, 2011.

White, D. C., Davis, W. M., Nickels, J. S., King, J. D., and Bobbie, R. J.: Determination of the sedimentary microbial biomass by extractible lipid phosphate, Oecologia, 40, 51–62, https://doi.org/10.1007/BF00388810, 1979.

Wörmer, L., Lipp, J. S., Schröder, J. M., and Hinrichs, K.-U.: Application of two new LC–ESI–MS methods for improved detection of intact polar lipids (IPLs) in environmental samples, Org. Geochem., 59, 10–21, https://doi.org/10.1016/j.orggeochem.2013.03.004, 2013.

Wörmer, L., Lipp, J. S., and Hinrichs, K.-U.: Comprehensive Analysis of Microbial Lipids in Environmental Samples Through HPLC-MS Protocols, in: Hydrocarbon and Lipid Microbiology Protocols, edited by: McGenity, T. J., Timmis, K. N., and Nogales, B., Springer Berlin Heidelberg, Berlin, Heidelberg, 289–317, https://doi.org/10.1007/8623_2015_183, 2015.

Wu, W., Xu, Y., Hou, S., Dong, L., Liu, H., Wang, H., Liu, W., and Zhang, C.: Origin and preservation of archaeal intact polar tetraether lipids in deeply buried sediments from the South China Sea, Deep-Sea Res. I: Oceanogr. Res. Pap., 152, 103107, https://doi.org/10.1016/j.dsr.2019.103107, 2019.

Xiao, W., Wang, Y., Zhou, S., Hu, L., Yang, H., and Xu, Y.: Ubiquitous production of branched glycerol dialkyl glycerol tetraethers (brGDGTs) in global marine environments: a new source indicator for brGDGTs, Biogeosciences, 13, 5883–5894, https://doi.org/10.5194/bg-13-5883-2016, 2016.

Xie, S., Lipp, J. S., Wegener, G., Ferdelman, T. G., and Hinrichs, K.-U.: Turnover of microbial lipids in the deep biosphere and growth of benthic archaeal populations, Proc. Natl. Acad. Sci. U.S.A., 110, 6010–6014, https://doi.org/10.1073/pnas.1218569110, 2013.

Xie, S., Liu, X.-L., Schubotz, F., Wakeham, S. G., and Hinrichs, K.-U.: Distribution of glycerol ether lipids in the oxygen minimum zone of the Eastern Tropical North Pacific Ocean, Org. Geochem., 71, 60–71, https://doi.org/10.1016/j.orggeochem.2014.04.006, 2014.

Yang, H., Pancost, R. D., Tang, C., Ding, W., Dang, X., and Xie, S.: Distributions of isoprenoid and branched glycerol dialkanol diethers in Chinese surface soils and a loess–paleosol sequence: Implications for the degradation of tetraether lipids, Org. Geochem., 66, 70–79, https://doi.org/10.1016/j.orggeochem.2013.11.003, 2014.

Yoshinaga, M. Y., Kellermann, M. Y., Rossel, P. E., Schubotz, F., Lipp, J. S., and Hinrichs, K.: Systematic fragmentation patterns of archaeal intact polar lipids by high-performance liquid chromatography/electrospray ionization ion-trap mass spectrometry, Rap. Comm. Mass Spectrom., 25, 3563–3574, https://doi.org/10.1002/rcm.5251, 2011.

Zhang, T., He, W., Liang, Q., Zheng, F., Xiao, X., Zeng, Z., Zhou, J., Yao, W., Chen, H., Zhu, Y., Zhao, J., Zheng, Y., and Zhang, C.: Lipidomic diversity and proxy implications of archaea from cold seep sediments of the South China Sea, Front. Microbiol., 14, 1241958, https://doi.org/10.3389/fmicb.2023.1241958, 2023.

Zhang, Y. G., Zhang, C. L., Liu, X.-L., Li, L., Hinrichs, K.-U., and Noakes, J. E.: Methane Index: A tetraether archaeal lipid biomarker indicator for detecting the instability of marine gas hydrates, Earth. Planet. Sci. Lett., 307, 525–534, https://doi.org/10.1016/j.epsl.2011.05.031, 2011.

Zhang, Y. G., Pagani, M., and Wang, Z.: Ring Index: A new strategy to evaluate the integrity of TEX_{86} paleothermometry, Paleoceanography, 31, 220–232, https://doi.org/10.1002/2015PA002848, 2016.

Zorz, J., Li, C., Chakraborty, A., Gittins, D. A., Surcon, T., Morrison, N., Bennett, R., MacDonald, A., and Hubert, C. R. J.: *SituSeq*: an offline protocol for rapid and remote Nanopore 16S rRNA amplicon sequence analysis, ISME Commun., 3, 33, https://doi.org/10.1038/s43705-023-00239-3, 2023.